Speleothems Reveal 500,000-year History of Siberian Permafrost

Speleothems reveal 500,000-year history of Siberian permafrost

Vaks, A.*, Gutareva, O.S., Breitenbach, S.F.M., Avirmed, E., Mason, A.J., Thomas, A.L., Osinzev, A.V., Kononov, A.M., & Henderson, G.M.

*Corresponding Author

Email anton.vaks@earth.ox.ac.uk

Speleothems reveal 500 kyr history of Siberian permafrost

Vaks, A.[1]*, Gutareva, O.S.[2], Breitenbach, S.F.M.[3], Avirmed, E.[4], Mason, A.J.[1], Thomas, A.L.[1], Osinzev, A.V.[5], Kononov, A.M.[2], & Henderson, G.M.[1]

Soils in permafrost regions contain twice as much carbon as the atmosphere, and permafrost has an important influence of the natural and built environment at high northern latitudes. There is little information about how permafrost responded to glacial-interglacial transitions and to global temperatures warmer than present. In this study, we date periods of speleothem growth in a north-south transect of caves in Siberia to reconstruct the history of permafrost in past climate states. Speleothem growth is restricted to full interglacial conditions in all studied caves. In the northernmost cave (at 60^{o}N), no growth has occurred since Marine Isotopic Stage (MIS) 11. Growth at that time indicates that global climates only slightly warmer than today are sufficient to thaw significant regions of permafrost.

Permafrost regions (where the ground is frozen for at least two consecutive winters and the intervening summer) cover 24% of the northern-hemisphere land surface and hold ≈1700 Gt of organic carbon. When it thaws it releases CO_2 and CH_4, turning a long-term carbon sink into a source and enhancing the greenhouse effect (*1-2*). Permafrost degradation also intensifies thermo-karst development, coastline erosion and liquefaction of ground previously cemented by ice. The latter endangers infrastructure including major Siberian oil and gas facilities (*3*). An ability to predict the extent of future permafrost degradation is desirable.

Assessing the response of permafrost to changing climate is challenging. Significant warming and thawing of local permafrost settings are seen in instrumental records during the last 20 years (*4*) but permafrost extent on continental scale is slow to respond to warming. For the latter, spatially distributed and long term data is still sparse. To understand the long-term response of permafrost to climate change requires knowledge of past permafrost conditions. Dating of organic material (*4*) or ground ice (*5*) can indicate the age of existing permafrost, but cannot reveal the longer-term history of permafrost.

In this study, we use cave carbonates (speleothems) as a tool to date past permafrost and its relationship to global climate. Vadose speleothems (stalactites, stalagmites and flowstones) form when meteoric waters (i.e. water originating from atmospheric precipitation) seep through the

vadose zone into caves. Cave temperatures usually approximate the local mean annual air temperatures (MAAT), because of buffering by the surrounding rock (*6*). When cave temperatures drop below 0°C, waters freeze and speleothem growth ceases. Speleothems found in modern permafrost regions are therefore relicts from warmer periods before permafrost formed (*7-9*). Absence of water also prevents speleothem growth in arid settings, so speleothem growth episodes in modern deserts are proxies for past wet periods (*10*). Because speleothems can be robustly and precisely dated with U-Th techniques, they provide a detailed history of periods when liquid water was available, and both permafrost and desert conditions were absent.

We reconstruct the history of Siberian permafrost (and the aridity of the Gobi Desert) during the last ~500 kyr using U-Th dating of speleothems in six caves along a north-south transect in northern Asia from Eastern Siberia at 60.2°N to the Gobi Desert at 42.5°N (Fig. 1). The northernmost cave - Lenskaya Ledyanaya sits today on the boundary of continuous permafrost with MAAT substantially below 0°C (*11*). The permafrost type changes to the south-west to discontinuous, sporadic, and then to permafrost-free conditions (*12*) (Fig. 1). Annual precipitation in this Siberian region is 400-600 mm/y falling mainly during summer. To the south, in the Gobi, MAAT ranges from +2°C to +8°C and little precipitation falls (200-80 mm/y) (*13*).

Speleothem thickness provides an indication of long-term liquid-water availability along the transect. Only 8 cm of growth is seen in the northernmost cave, increasing to ~70 cm in the caves of southern Siberia and decreasing again to less than 30 cm in the Gobi. As expected, southern Siberia is more suitable for speleothem growth than the cold north or the dry south. All recovered speleothems show a texture of calcium-carbonate layers alternating with growth hiatuses (see Supporting Online Material; SOM).

Thirty-six speleothems were collected from the caves and 111 U-Th ages conducted (Fig 2A). In each speleothem, at least one sample was taken from the outermost layer and from each section of growth (i.e. between hiatuses) inward, until the limits of the U-Th chronology were reached (~500 ka) to assess all periods of growth. A full description of the samples, and their sub-sampling and dating is given in the SOM.

The youngest speleothem growth in the region of modern continuous permafrost (i.e. at 60°N) occurred during interglacial MIS-11, contrasting with the centre of the transect where speleothems grew during all interglacials (Fig. 2A, B). Age ranges in southern Siberia also

demonstrate that the duration of speleothem deposition in MIS-11 was longer than during subsequent interglacials. These observations indicate that permafrost thawing during MIS-11 was more extensive than at any other point during the last 450 kyr and extended northward of 60°N, significantly further north than the present limit of continuous permafrost. Some similar thawing may also have occurred at MIS-13 in this most northerly cave. The absence of any observed speleothem growth since MIS 11 in the northerly Lenskaya Ledyanaya cave (despite dating outer edges of 7 speleothems), suggests the permanent presence of permafrost at this latitude since the end of MIS-11. Speleothem growth in this cave occurred in early MIS-11, ruling out the possibility that the unusual length of MIS-11 caused the permafrost thawing.

MIS-11 was also characterized by wetter conditions in the Mongolian Gobi Desert, as shown by two ages from Shar-Khana Cave speleothems (Fig. 2A), which contrast with the absence of growth during subsequent interglacials. The existence of a humid event in the Gobi during early MIS-11 is supported by mollusk assemblages from Chinese Loess Plateau (*14*), and by the dominance of input into Lake Baikal via the Selenga River during MIS-11 (*15*).

The degradation of permafrost at 60°N during MIS-11 allows an assessment of the warming required globally to cause such extensive change in the permafrost boundary. There is significant evidence that MIS-11 was the warmest of recent interglacials, including the presence of boreal forest on South Greenland at that time (*16*), the absence of ice-rafted debris in the North Atlantic (*17*), increased sea levels (*18*), and higher sea-surface temperatures (SST) in the tropical Pacific (*19-21*). Mg/Ca reconstructions (*20-21*) indicate that SST of the Pacific Warm Pool (PWP) reached >30°C in early MIS-11, compared to 29.5°C in MIS-5.5 and ~28.5°C during the pre-industrial Late Holocene (Fig. 2D). This tropical heat was transported poleward (*22*) and there is evidence of unusual warmth in Siberia during MIS-11, evidenced by the high fraction of biogenic silica in the sediments of Lake Baikal (*23*) (Fig. 2C) and high spruce pollen content in Lake El'gygytgyn, suggesting local temperatures 4-5°C above present (*24*). When PWP temperatures reach 30°C this appears to cause more pronounced warming of northern continents, and lead to significant northward migration of the permafrost boundary.

Periods of Siberian speleothem growth since MIS-11 suggest a close link between greenhouse warming/global temperatures and permafrost extent. After a brief post MIS-11 hiatus in growth (from 370 to 355 ka), coinciding with a minimum in atmospheric CO_2 and in PWP SST during MIS-10 (Fig. 2D, F), significant thicknesses of speleothem grew in Southern Siberia during MIS-

9 as greenhouse gases returned to higher values. Speleothems also grew actively during MIS-5.5 and the Holocene (>5 cm) when CO_2 levels were high. In contrast, growth during MIS-7, a period of lower CO_2 and cooler global conditions, is minimal (maximum 1.5 cm in any studied cave) and no growth is observed during MIS-5.4 to 5.1. Conditions during MIS-7 were at the very limit for growth in southern Siberia: speleothems grew during MIS-7.3 and 7.1 in Okhotnichya Cave (52^oN) but only during MIS-7.1 just to the north at Botovskaya Cave (55^oN). No growth occurred during MIS-7.5 at either cave despite higher concentrations of CO_2 and CH_4 than later in MIS-7 (*25-26*) and high PWP SST (Fig 2D-F) (*20-21*). Lake Baikal biogenic silica (*23*) and the percentage of arboreal pollen in Lake El'gygytgyn sediments (*27*) are also lower during MIS-7.5 than during MIS-7.3 and 7.1. Lower local summer insolation during MIS-7.5 (Fig 2G) (*28*) suggests a role for local insolation in overprinting a Siberian climate dominantly controlled by global greenhouse gas levels.

U-Th dating of Siberian speleothem growth during recent interglacials allows detailed comparison of permafrost history with other aspects of the global climate system (Fig 3). During MIS-5.5, speleothems started growing between 128.7 and 127.3 ka, and ended between 119.2 and 118.1 ka (determined from Bayesian analysis of U-Th data using OxCal-4.1; see SOM for details). The permafrost thawing initiated when insolation was close to its maximum and greenhouse gases had just reached maximum values. Holocene permafrost degradation in our sites lags maximum insolation and greenhouse gas concentrations slightly, and starts between 10.0 and 9.8 ka. This lag may be due to the time required for permafrost to thaw at the slightly lower insolation and CO_2 levels of the Holocene (relative to MIS-5.5).

Overall, dated periods of speleothem growth allow an assessment of the relationship between global temperature and permafrost extent. PWP SST was 0.5-1.0°C higher during MIS-5.5 and ≈1.5°C higher during early MIS-11 relative to the pre-industrial Late Holocene (Fig. 2D) (*20-21*). Using PWP SST as a surrogate for global temperature (*20*) suggests that increase in global temperatures by 0.5-1.0°C will degrade only non-continuous permafrost in southern Siberia with the Gobi Desert remaining arid. Warming of ≈1.5°C (i.e. as in MIS-11) may cause a substantial thaw of continuous permafrost as far north as 60°N, and create wetter conditions in the Gobi Desert. Such warming is therefore expected to dramatically change the environment of continental Asia, and can potentially lead to substantial release of carbon trapped in the permafrost into the atmosphere.

Acknowledgments

This article is dedicated to the memory of Prof. Y. Trzhcinski, who during the last months of his life made a big effort to establish the cooperation between University of Oxford and Institute of Earth's Crust (IEC) in Irkutsk. Thanks to D. Sokolnikov and other 'Arabica' members, E. Kozireva (IEC), V. Alexioglo and V. Balaev from Lensk for their help during the fieldwork in Siberia, Mongolian Speleological Society for their help with the fieldwork in Mongolia; to J. Fritz and L. Zehnder (ETH Zurich) for drawing Fig. 1 and for assistance with XRD analyses respectively; to C. Day, V. Ersek, P. Holdship, O. Green, S. Wyatt, Y. Nakajima, P. Pousada Solino and others from University of Oxford for the help with the laboratory work, administration issues and fruitful discussions. This work was funded by NERC Fellowship NE/G013829/1, Royal Society grant JP080831 and Russian Foundation for Basic Research joint grant 09-05-92605 KO_a.

References and Notes:

1. G. Grosse, V. Romanovsky, *EOS* 92, 73 (2011).
2. E. A. G. Schuur *et al.*, *BioScience* 58, 701 (2008).
3. O. Anisimov, S. Reneva, *AMBIO: A Journal of the Human Environment* 35, 169 (2006).
4. Y. K. Vasil'chuk, J.-C. Kim, A. C. Vasil'chuk, *Nuclear Instruments and Methods in Physics Research Section B: Beam Interactions with Materials and Atoms* 223-224, 650 (2004).
5. D. A. Gilichinsky *et al.*, *Quaternary Science Reviews* 26, 1547 (2007).
6. H. P. Schwarcz, in *Handbook of Environmental Isotope Geochemistry*, P. Fritz, J. C. Fontes, Eds. (Elsevier, Amsterdam, 1986), vol. 2, pp. 271-300.
7. R. A. Cliff, C. Spötl, A. Mangini, *Quaternary Geochronology* 5, 452 (2010).
8. B. Lauriol, D. C. Ford, J. Cinq-Mars, W. A. Morris, *Canadian Journal of Earth Sciences* 34, 902 (1997).
9. S. E. Lauritzen, *Quaternary Research* 43, 133 (1995).
10. A. Vaks, M. Bar-Matthews, A. Matthews, A. Ayalon, A. Frumkin, *Quaternary Science Reviews* 29, 2647 (2010).
11. Philip's, Ed., *Modern School Atlas, 95-th edition*, (Philip's, a division of Octopus Publishing Group Limited, London, 2007).

12. A. Jones *et al.*, Eds., *Soil Atlas of the Northern Circumpolar Region*, (European Commission, Publication Office of the European Union, Luxembourg, 2010), pp. 144.
13. D. Dorjotov, N. Orshikh, T. Oyunchimeg, *Geographic Atlas of Mongolian Republic (in Mongolian)*. (Mongolian Institute of Geodesy and Cartography Ulaanbaatar, Mongolia, 2004), pp. 64.
14. N. Wu *et al.*, *Quaternary Science Reviews* 26, 1884 (2007).
15. A. W. Mackay *et al.*, *Journal of Quaternary Science* 23, 365 (2008).
16. A. de Vernal, C. Hillaire-Marcel, *Science* 320, 1622 (2008).
17. J. F. McManus, D. W. Oppo, J. L. Cullen, *Science* 283, 971 (1999).
18. M. E. Raymo, J. X. Mitrovica, *Nature* 483, 453 (2012).
19. L. Ortlieb, A. Diaz, N. Guzman, *Quaternary Science Reviews* 15, 857 (1996).
20. J. Hansen *et al.*, *Proceedings of the National Academy of Sciences* 103, 14288 (2006).
21. M. Medina-Elizalde, D. W. Lea, *Science* 310, 1009 (2005).
22. A. J. Dickson *et al.*, *Nature Geosci* 2, 428 (2009).
23. A. A. Prokopenko *et al.*, *Quaternary Research* 55, 123 (2001).
24. M. Melles *et al.*, *Science* 337, 315 (2012).
25. L. Loulergue *et al.*, *Nature* 453, 383 (2008).
26. D. Luthi *et al.*, *Nature* 453, 379 (2008).
27. N. R. Nowaczyk *et al.*, *Geophysical Journal International* 150, 109 (2002).
28. J. Laskar *et al.*, *Astronomy and Astrophysics* 428, 261 (2004).
29. J. Brown, J. O. J. Ferrians, J. A. Heginbottom, E. S. Melnikov. (National Snow and Ice Data Center/World Data Center for Glaciology. Digital media., Boulder, CO, 2001).
30. L. E. Lisiecki, M. E. Raymo, *Paleoceanography* 20, (2005).
31. Y. Wang *et al.*, *Nature* 451, 1090 (2008).
32. S. O. Rasmussen *et al.*, *J. Geophys. Res.* 111, D06102 (2006).
33. See references 16-19 in Supporting online material.

Figure Captions:

Figure 1: Map showing the extent of permafrost types in eastern Siberia, the Gobi Desert, and the location of studied caves (black circles). Permafrost data is taken from Brown et al. (2001) (*29*).

Figure 2: (A) Distribution of speleothem U-Th ages (±2□□ in time and space; *n* – total number of U-Th age determinations per cave, including those beyond the U-Th range) with grey bars signifying periods of growth in Okhotnichya and Botovskaya caves. (B) Benthic □ ^{18}O stack (*30*) with MIS numbers. (C) Concentration of biogenic silica in Lake Baikal sediments (%) (*23*). (D) Pacific Warm Pool Mg/Ca SST, with the pre-industrial Late Holocene SST shown by red horizontal fragmented line (*20-21*). (E, F) CH_4 and CO_2 records of EPICA Dome C respectively (*25-26*). (G) Summer insolation at 55°N (*28*). Speleothems with ages exceeding 500 ka (within ±2□□ range) are not shown, but accounted for in *n*. Two samples SLL9-2-A+B and SOP-32-B are not included because they reflect a mixture of material from different layers; please refer to the Supplementary Table 1.

Figure 3: Siberian speleothem growth periods during Holocene and MIS-5.5 (A) with grey bars indicating periods of growth. Compared with East-Asian Monsoon record from Hulu and Sanbao caves (B) (*31*), GICC05 □ ^{18}O (C) (*32-33*), CH_4 (D) and CO_2 (E) records of EPICA Dome C (*25-26*), and 55°N summer insolation (F) (*28*).

Figure 1.

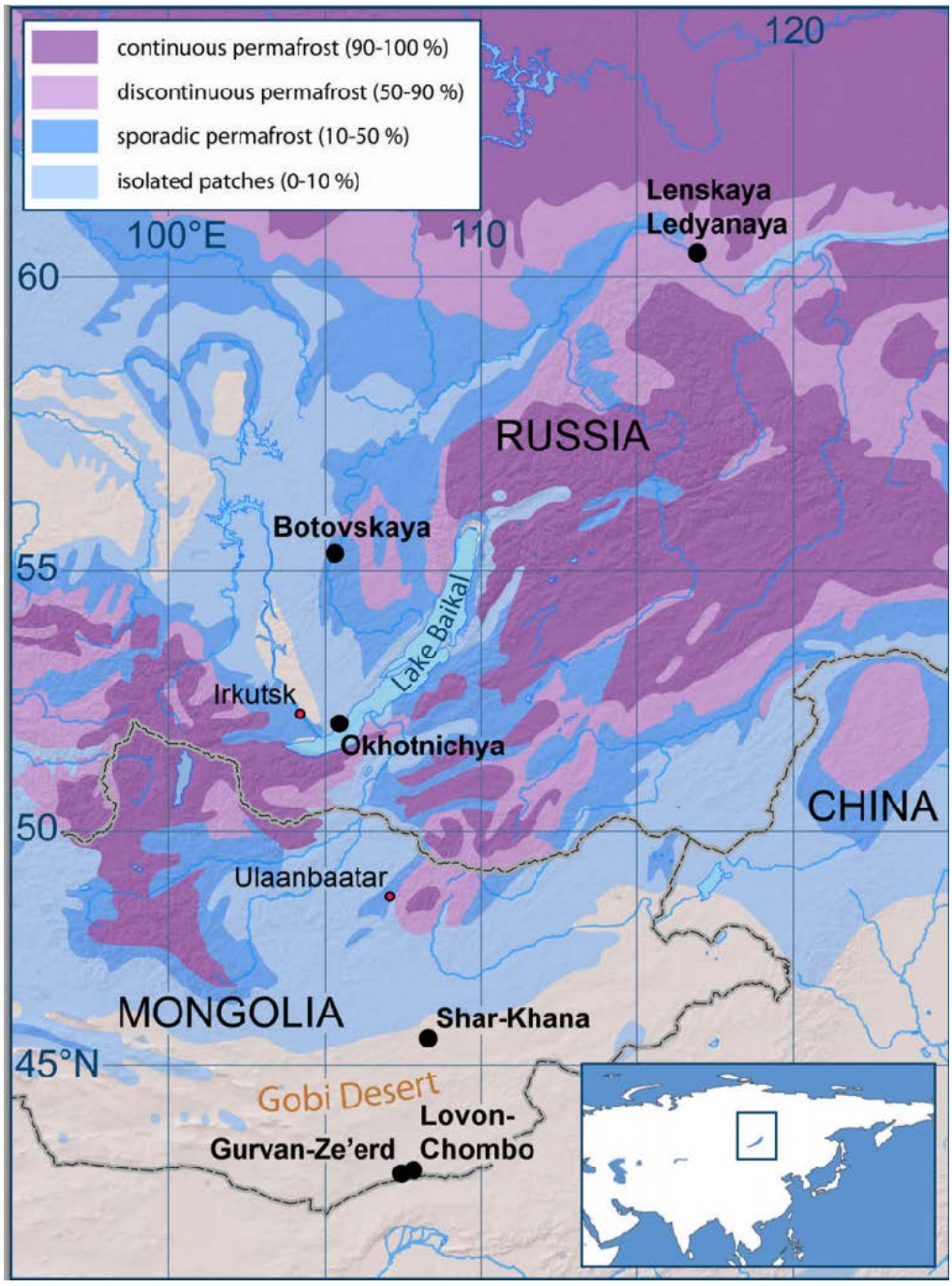
continuous permafrost (90-100 %)
discontinuous permafrost (50-90 %)
sporadic permafrost (10-50 %)
isolated patches (0-10 %)
120
100°E
110
60
55
50
45°N
Lenskaya
Ledyanaya
RUSSIA
Botovskaya
Lake Baikal
Irkutsk
Okhotnichya
CHINA
Ulaanbaatar
MONGOLIA
Shar-Khana
Gobi Desert
Lovon-
Gurvan-Ze'erd
Chombo

Figure 2.

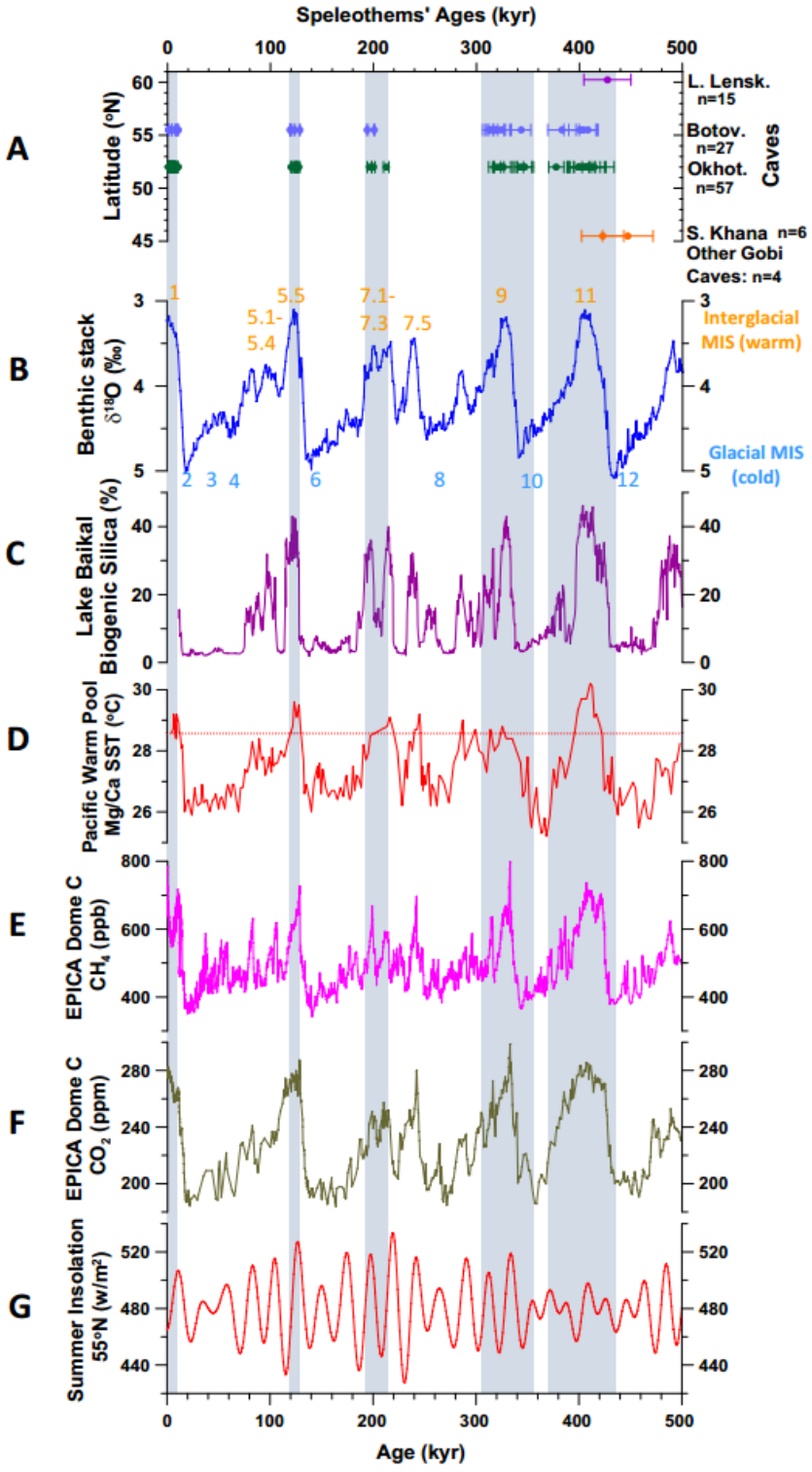
Speleothems' Ages (kyr)
A
Latitude (°N)
L. Lensk. n=15
Botov. n=27
Okhot. n=57
Caves
S. Khana n=6
Other Gobi Caves: n=4
B
Benthic stack δ18O (‰)
Interglacial MIS (warm)
Glacial MIS (cold)
C
Lake Baikal Biogenic Silica (%)
D
Pacific Warm Pool Mg/Ca SST (°C)
E
EPICA Dome C CH4 (ppb)
F
EPICA Dome C CO2 (ppm)
G
Summer Insolation 55°N (w/m²)
Age (kyr)

Figure 3.

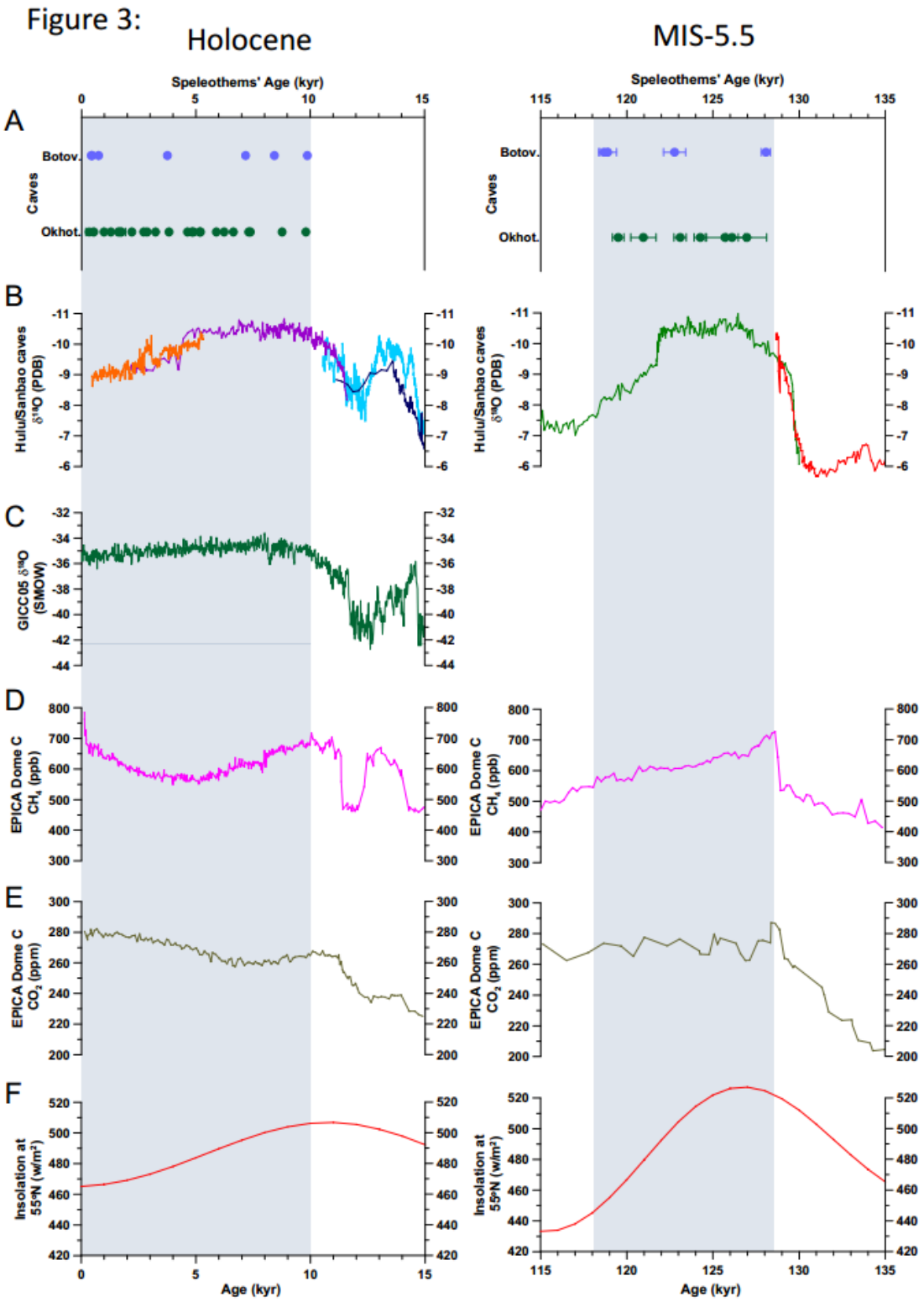
Figure 3:
Holocene
MIS-5.5
Speleothems' Age (kyr)
A
Caves
Botov.
Okhot.
B
Hulu/Sanbao caves δ18O (PDB)
C
GICC05 δ18O (SMOW)
D
EPICA Dome C CH4 (ppb)
E
EPICA Dome C CO2 (ppm)
F
Insolation at 55°N (w/m²)
Age (kyr)